RECEIVED
CENTRAL FAX CENTER
SEP 19 2005

RADER, FISHMAN & GRAUER PLLC

Worldwide Intellectual Property Matters • Patents • Trademarks
Litigation • Copyrights • U.S. and Foreign Portfolio Management
Computer and Internet Law • Trade Secrets • Unfair Competition

To:	Examiner Dennis Rosario-Vasques	**From:**	Alexander Rabinovich
Fax:	703-872-9306	**Pages:**	5 + Coversheet
Phone:		**Date:**	September 19, 2005
Re:	09/786,477	**cc:**	

☐ **Urgent** ☒ **For Review** ☐ **Please Comment** ☐ **Please Reply** ☐ **Please Recycle**

• **Comments: Per our conversation, please see the attached cited reference that we submitted on 5/2/2001**

39533 Woodward Ave., Suite 140 • Bloomfield Hills, MI 48304 • 248-594-0600 • Fax 248-594-0610 • www.raderfishman.com
Bloomfield Hills Washington, D.C. Salt Lake City Tokyo

Technical Note

Vessel Enhancement Filtering in Three-Dimensional MR Angiograms Using Long-Range Signal Correlation

Yiping P. Du, PhD • Dennis L. Parker, PhD

Small vessels in three-dimensional MR angiograms have low visibility in maximum-intensity projection images because of their low contrast. In a previous study, we had two nonlinear filters that appeared to give significant improvement in small vessel detail. In this paper, we report on a generalization of this filter that allows a more general modeling of the vessels and a more complete suppression of background. One implementation of the general filter gave a vessel mean contrast-to-noise ratio that is 2.52 and 3.51 times higher than the vessel mean contrast-to-noise ratio obtained using our previously reported maximum-minimum (max-min) filter and cross- section filter, respectively.

Index terms: Contrast enhancement • Image filtering • Image processing • Vascular studies • Interpolation

JMRI 1997; 7:447–450

Abbreviations: MRA = MR angiogram, TOF = time-of-flight, MIP = maximum-intensity projection, CNR = contrast-to-noise ratio, ZFI = zero-filled interpolation, SD = second difference

From the Department of Radiology, University of Utah Health Sciences Center, 50 North Medical Drive, Salt Lake City, UT 84132. Received June 11, 1996; accepted September 19, 1996. This study was presented in part at the third Annual Meeting of the Society of Magnetic Resonance, Nice, France, August 19-25, 1995. This study was supported in part by National Institutes of Health R01HL 48223 and a Technology Innovation Grant from the University of Utah Research Foundation. Address reprint requests to Y.P.D. at GE Medical Systems, P.O.Box 414, W-827, Milwaukee, WI 53201.

THIS PAPER IS A CONTINUATION of our studies to use image processing techniques to improve small vessel visibility in magnetic resonance angiography (MRA). In time-of-flight (TOF) MRA techniques, vessel signal is low in small vessels, where the slowly flowing blood experiences many excitation pulses. The vessel-background contrast of small vessels is further reduced by the use of the maximum-intensity projection (MIP) algorithm (1–4).

Limited improvements in vessel visibility have been obtained by using different digital filters (5–7) and other postprocessing techniques (8–10). The development of more effective filters will be necessary before the filtering technique can be used to improve clinical diagnoses.

We have recently reported on two nonlinear, anisotropic, digital vessel-enhancement filters (11,12) that were developed based upon the characteristics of small vessels in a nearly uniform background signal distribution and upon the properties of a second difference operator. The filters were designed based on a line- segment model in which a small vessel is approximated as a sequence of voxels (ie, a line segment) with higher signal intensity than the surrounding background. Although these filters were shown to improve significantly the visibility of small vessels, both filters tend to increase image noise, in spite of the efforts that were made to suppress noise in the design of the filters.

In this paper, we employ a more general vessel model that approximates the vessel as a cylinder segment of finite width. This model can be used to design a family of filters that are optimized to enhance vessels of specific sizes and suppress noise and signal from stationary tissue. We demonstrate that one of our previous filters is a nonoptimized specific example from this family of filters. Based upon this generalized model and our knowledge of the image point spread function, we have developed a more optimal nonlinear, anisotropic vessel-enhancement filter that uses long-range signal correlation and is designed to enhance vessels of the smallest diameters that can be observed in our MRA images. Quantitative contrast-to-noise-ratio (CNR) measurements have been used to assess the improvement of vessel visibility obtained by using the proposed filter compared with our previously reported filters.

• THEORY

Modeling of Three-Dimensional MRA Image

Our generalized filter is based upon the signal properties in the three-dimensional TOF MRA images, where flowing blood experiences fewer RF excitation pulses and therefore has higher signal intensity than the surrounding background that is highly saturated and exhibits very little spatial variation. Image noise consists of randomly distributed intensity variations over the entire image. Furthermore, the filter also takes advantage of the improved CNR, continuity and smoothness of small vessels that results from zero-filled interpolation (ZFI) (13–16). We believe that ZFI of MRAs is a critical step to ensure the success of subsequent vessel enhancement filtering techniques (11,12).

In ZFI interpolated image data sets, the image point spread function is about the same width as the interpolation factor, and the cross-section of a small vessel is represented by multiple grid points. Therefore, the line model in Figure 1 does not adequately represent a small vessel when the three-dimensional angiograms have been interpolated before the filtering process (12). We model a small vessel as a cylinder that contains voxels with higher intensity than background. In a plane containing the vessel cross-section, the voxels in the center of the cylinder have the highest signal intensity compared with the voxels close to the edge of (but still within) the cylinder. We model the stationary tissue as a constant background and assume that the correlation of image noise is negligible from voxel to voxel.

In our previous ZFI studies (17,18), we used the interpolation factor, L, to describe the power of magnification in the matrix dimension. For instance, the interpolation from a 256 × 256 × 32 to 1024 × 1024 × 128 has L = 4. We found that in a three-dimensional MRA interpolated using ZFI with an interpolation factor of L, the apparent diameter of the smallest visible vessels is about 2L−1 pixels. Therefore, this cylinder model would appear to be correct for even the smallest vessels in

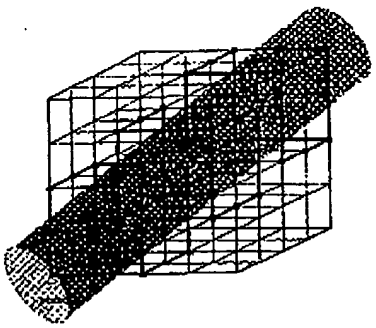

Figure 1. Schematic shows the orientation correlation of a small vessel between three neighboring 3 × 3 × 3 cubes (K = 1). Each of the arrows represents the direction in which $g_{i,M}$ has the maximum value in this 3 × 3 × 3 cube.

the interpolated MR angiograms. Given this observation, we would propose that an efficient filter (one that gives good vessel enhancement and soft tissue suppression) will approximate the properties of the desired vessel limited by the imaging point spread function.

A Simple Generalized Filter

To test our model, we have implemented an approximation of the desired filter for which the coefficients consist of three positive central points and two negative points at an appropriate distance from the central points. This vessel enhancement filter, which is applied to the three-dimensional image data before MIP reconstruction, utilizes the 13 discrete directions that pass through the center of a three-dimensional cube with 3 voxels on each side (see second figure in Du et al. [12]). These 13 discrete directions can be written in Cartesian coordinate as: (1, 0, 0), (0, 1, 0), (0, 0, 1), (1, 1, 0), (1, −1, 0), (1, 0, 1), (1, 0, −1), (0, 1, 1), (0, −1, 1), (1, 1, 1), (1, −1, 1), (1, 1, −1), and (1, −1, −1). The algorithm begins by applying a long-range differential operator, D_M, along each of these 13 discrete directions. The D_M operator at an image point i and operating along a discrete direction $\vec{j}$ is defined as:

$$D_{i,M} = 2f_i + f_{i-j} + f_{i+j} - 2f_{i-M} - 2f_{i+M} \quad (1)$$

where f_i is the image intensity at point i, f_{i-j} and f_{i+j} are the image intensities at the neighboring points of f_i along direction $\vec{j}$, and M is the signal correlation range of the operator. The second difference (SD) operator, used in Du et al. (12) is a special case of D_M when M = 1.

Based on the cylinder model described above, the D_M operator has the following properties, which are essentially identical to those considered in our previous filter design (12): 1) At a point centered on a vessel, the D_M operator has a large positive value in a direction perpendicular to the vessel ($\vec{j}_n$ in Fig. 2) and a small positive or negative value in the direction parallel to the vessel ($\vec{j}_v$ in Fig. 2); 2) At a point near the vessel edge, the D_M operator has a large negative value in a direction perpendicular to the vessel edge ($\vec{j}_e$ in Fig. 2) and a small positive or negative value in the direction parallel to the vessel ($\vec{j}_v$ in Fig. 2); 3) In background regions with small intensity variations, the D_M operator has a small value, either positive or negative, in all directions; 4) Finally, the D_M operator has large positive values in all directions on positive noise spikes and large negative values in all directions on negative noise spikes. Using these properties of the D_M operator, we have designed a family of filters (with different correlation ranges) to reduce image background, enhance vessel structures, and suppress noise spikes.

The D_M operator enhances cylindrical structures with diameter of $(2M-1)$ grid points or smaller. The D_M operator is then used to construct a g_M operator, similar to using the SD operator to construct a cross-section filter:

$$g_{i,M} = \frac{1}{N}\sum_{n=1}^{N} D^n_{i,M} - \max(0, D_{i,M}) \quad (2)$$

where N is the number of discrete directions that are perpendicular to $\vec{j}$, and $D^n_{i,M}$ is denoted to the D_M operator at point i along a direction perpendicular to $\vec{j}$.

The maximum value of $g_{i,M}$ over the 13 discrete directions provides an estimate of whether the image voxel is vessel or nonvessel. If this image voxel is vessel, the vessel is most likely in the direction $\vec{j}$ at which $g_{i,M}$ has the maximum value (see Fig. 1). Instead of using $g_{i,M}$ to construct a filter similar to the cross-section filter, we designed a filter using the relationship between $g_{i,M}$ and the orientation of vessels. In the design of the filter, we also assumed that the small vessel has a strong orientation-dependent correlation within a small cubic volume of $[2(M + K) - 1] \times [2(M + K) - 1] \times [2(M + K) - 1]$ voxels. The filter with signal correlation range of M and orientation-dependent correlation range of K is given by:

$$G^K_M(i) = \max_{j=1,\ldots,13}\left(\sum_{k=-K}^{K} g_{i+k\vec{j},M}\right) \quad (3)$$

where $\sum_{k=-K}^{K} g_{i+k\vec{j},M}$ is the summation of $g_{i,M}$ along the direction of $\vec{j}$.

For the visualization of the smallest vessels in a three-dimensional MRA image data set with an interpolation factor of L, we tested the values of $M = L$ and $K = L - 1$. These values arise because of the expected correlation distance of $2L - 1$ that arises from the interpolation process. The chosen values allow averaging over the expected correlation distance and the SD to be taken over a distance that is just greater.

• METHODS

To test the vessel enhancement filtering techniques, a three-dimensional single slab TOF MRA image was acquired on a conventional GE Signa MR Scanner (GE-Medical Systems, Milwaukee, WI) that operates at 1.5 Tesla. To reduce echo time,

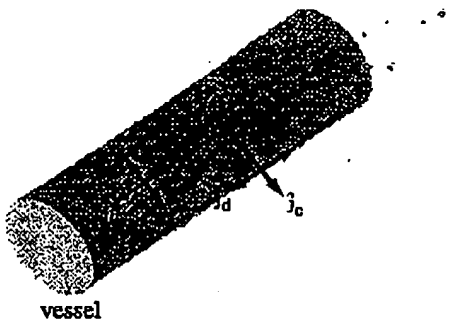

Figure 2. Schematic shows the location and direction that the differential operator D_M is applied. $\vec{j}_v$: on the vessel centerline, perpendicular to the vessel; $\vec{j}_e$: on the vessel centerline, along the vessel; $\vec{j}_e$: on the edge of the vessel, perpendicular to the vessel; $\vec{j}_n$: on the vessel centerline, along the vessel.

the readout was made asymmetric such that the echo center was placed at a point before the center of the readout window. For the studies of this paper, the shift was 25% of the total readout time. The circle of Willis was imaged in a 33-year-old human volunteer with the three-dimensional TOF technique (256 × 256 × 32 acquisition matrix, TR(msec)/TE(msec) = 48/7.0, 25° flip angle, 18-cm field of view, 0.75-mm section thickness).

In this study, we applied ZFI to increase the image matrix dimensions in all three directions by a factor of two (ie, L = 2) for the image data before filtering. After ZFI, three sets of filtered images were obtained by using the previously reported maximum-minimum and cross-section filters (11,12) and the new G^K_M filter with M = 2 and K = 1. The resulting image data were displayed using the MIP algorithm.

A vessel CNR measurement technique (19) was used to assess the CNR at each point along a vessel segment and the mean CNR of this vessel segment in these three-dimensional filtered data sets. Vessel contrast is the difference in image intensity between a vessel point and its surrounding nonvessel background. The standard deviation of image intensity in a three-dimensional region of background was used as the estimation of image noise for these three-dimensional filtered image data sets.

The G^1_2 filter has been implemented in the C language on a Sun™ Sparc 20 workstation (Sun Microsystems, Mountain View, CA). The computation time was 20 minutes for a 512 × 512 × 64 data set.

• RESULTS

The images of Figure 3 are all obtained from the same three-dimensional MRA image data. Figure 3a shows the MIP of the original 512 × 512 × 64 interpolated image. Figures 3b, c and d show the MIP images of the three-dimensional filtered image data sets using the maximum-minimum filter, cross-section filter, and the G^1_2 filter, respectively. Although there is

some variability in small vessel visibility between the images, it is evident that, in general, the small vessel detail is better and more continuous in Figure 3d. Figure 3 is a typical comparison of the effectiveness of these three filters in suppressing background signal and noise. In Figure 3, we found that the G_3^1 filter considerably improved the smoothness of vessels and reduced the noise level. We also found that the signal loss in large vessels was noticeably reduced by using the G_3^1 filter compared with that obtained using the maximum-minimum and cross-section filters.

Figure 4 plots the image intensity profile along a horizontal straight line across the posterior communicating arteries in the MIP images (as shown in Fig. 3a). The maximum intensity in each of the profile plots was normalized to 100. The intensity profiles on MIP images of the filtered three-dimensional image data sets show the vessel enhancement by using the maximum-minimum filter and the G_3^1 filter. Small vessels labeled as *G*, *H*, and *K* become visible in the MIP image of the maximum-minimum filtered data. In Figure 4a, we observe that the background signal was well suppressed. However, the noise level in background tissue and in air was increased. The plots in Figure 4b show that the G_3^1 filter suppresses background signal and noise more effectively compared with the maximum-minimum filter. The vessels labeled as *C*, *G*, *H*, and *K* have increased vessel-background contrast in the image processed using the G_3^1 filter compared with the image processed using the maximum-minimum filter.

Figure 5 illustrates the comparison of CNR measurements for three filtered image data sets. All of the vessels for which CNR could be conveniently measured were divided into 53 segments. These segments included large vessels, such as middle cerebral arteries, and the vessels barely visible in the local maximum-intensity projections. The mean CNR measurement obtained from these 53 vessel segments in the maximum-minimum filtered image data was plotted as the *x* axis. The mean CNR measurements from the same vessel segments in the image data sets processed using the cross-section filter and the G_3^1 filter were plotted along the *y* axis, respectively. In this figure, large vessel segments usually have high CNR values, and small vessel segments usually have low CNR values. The least-mean-square fit obtained using a linear function, $y = ax$, was performed for the mean CNR measurements. It was found from Figure 5 that the MRA processed using the G_3^1 filter has a considerable improvement in CNR compared with the same MR angiogram processed using the previously reported filters. In this study, the vessel mean CNR obtained using the G_3^1 filter was 2.52 and 3.51 times higher than the vessel mean CNR obtained using the maximum-minimum filter and cross-section filter, respectively.

• DISCUSSION

The results presented here substantiate our prediction that small vessel visibility will be improved by using a filter that matches the expected signal of the small vessels in the interpolated image data set. Although, as observed above, some small vessels may appear more visible in other processed images, in general, the simple implementation of our generalized filter (the G_3^1 filter) was found to considerably increase the visibility of small vessels and to suppress stationary background signal and image noise more effectively compared with our previously reported filters (12).

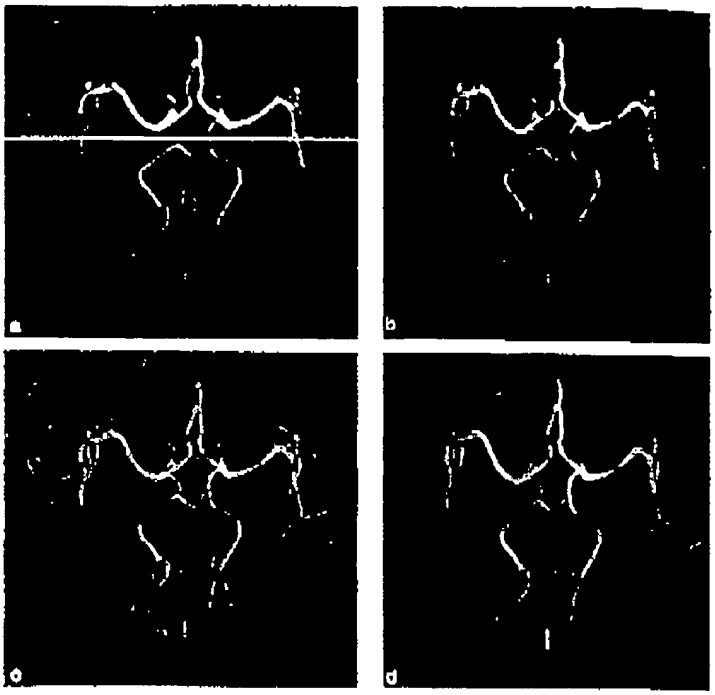

Figure 3. (a) The axial MIP image of a zero-filled-interpolated three-dimensional MRA image data set; (b) The MIP image of the filtered three-dimensional MRA data using a maximum-minimum filter; (c) The MIP image of the filtered three-dimensional MRA data using a cross-section filter; (d) The MIP image of the filtered three-dimensional MRA data using the G_3^1 filter. The same three-dimensional MRA data as in (a) was used as the original image data for these three filters.

Our modeling of small vessels in three-dimensional MRA data is based on the flow pattern of blood. The blood flow in a small vessel is usually fairly stable, so that this flow can be assumed to be laminar. In laminar flow, the fluid velocity has a parabolic distribution, with the maximum velocity at the center of the vessel and zero velocity at the edge of the vessel. In three-dimensional TOF MRA imaging techniques, faster flow experiences fewer radiofrequency excitations and has less signal saturation. Therefore, the signal contribution from the central part of the flow is higher than from the edge part of the flow. In the original image data sets, the image grid points are too coarse to show such signal distribution in small vessels. With ZFI, small vessels have a considerably improved CNR, continuity and smoothness. In a three-dimensional MRA with ZFI, the cross-section of a small vessel is represented by multiple voxels. After ZFI, especially when the interpolation factor is large, the signal distribution of a small vessel is much smoother in all directions compared with vessel smoothness in the original images. Realistic modeling of a small vessel in such interpolated images should treat a small vessel as a cylinder instead of a line that consists a sequence of high signal voxels. This cylinder has higher signal intensity along the center line and lower signal intensity close to the edge. For a small vessel, the diameter of this cylinder in number of grid points is approximately the same as the interpolation factor. The long range D_M operator was derived from this modeling of a small vessel.

As an example, a hypothetical signal intensity profile of a small vessel across the cross-section of the vessel is plotted in Figure 6a. At the center of this vessel, the SD operator has a value of 14 (= 2 × 130 − 123 − 123). The D_3 operator defined in Eq. [1] has a value of 60 (= 2 × 130 − 100 − 100) at the same location. This example shows the improved capability of enhancing small vessels using the G_3^1 filter.

In our previous studies, we observed that large vessel signal was decreased in general when the maximum-minimum and cross-section filters were used. In the current study, we also observed signal loss in large vessels, but this loss was apparently less than that from the other filters. In the G_3^1 filter, the D_M operator is sensitive to cylindrical structures with diameter of $2M - 1$ grid points, whereas the SD oper-

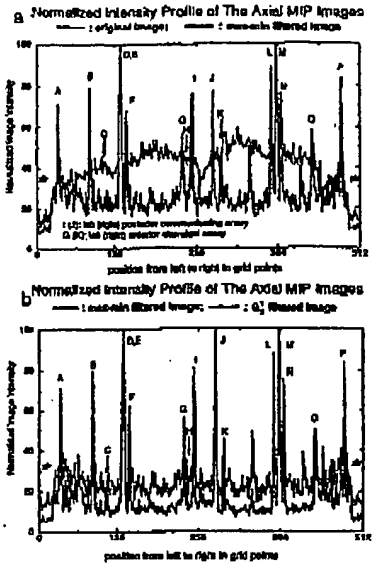

Figure 4. The comparison plots of image intensity profiles for the MIP images of (a) original image data and the maximum-minimum filtered image data; (b) the maximum-minimum filtered image data and the C^1_3 filtered image data.

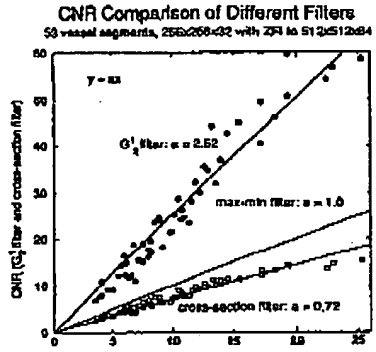

Figure 5. The mean CNR measurement of each of 53 vessel segments in an MRA processed using the G^1_3 filter and the cross-section filter as functions of the mean CNR measurement of the same vessel segments in the same MRA processed using the maximum-minimum filter.

ator in the maximum-minimum and cross-section filters is sensitive for line structures. Figure 6b shows a hypothetical signal intensity profile of a large vessel across the cross-section of the vessel. At the center of the vessel, the SD operator has a value of 8 (= 2 × 140 − 137 − 137), whereas the D_2 operator has a value of 20 (= 2 × 140 − 130 − 130). This explains why the G^1_3 filter has less signal loss in large vessels compared with the maximum-minimum and cross-section filters, as we found in our study.

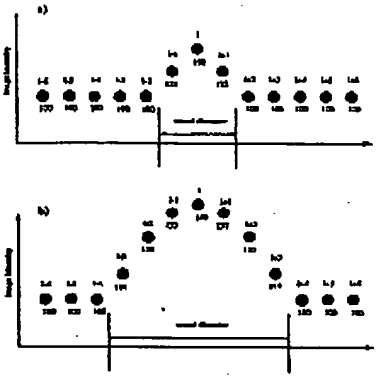

Figure 6. Hypothetical signal intensity profiles of a small vessel, (a), and a large vessel, (b), along the cross-sections of the vessels. In (a), the vessel center has a signal intensity of 130; the background has a signal intensity of 100. In (b), the vessel center has a signal intensity of 140; the background has a signal intensity of 100.

The G^1_3 filter is expected to have high sensitivity for vessels with diameter $2M-1$ grid points or smaller. If M in the G^1_3 filter is chosen to be larger than the interpolation factor, L, the G^1_3 filter is expected to have a better sensitivity for larger vessels. However, choosing M to be larger than L might slightly reduce the sensitivity for small vessels. Using a large K value also increases the computation time considerably. Therefore, we recommend using $M = L$ and $K = L - 1$ to avoid this signal loss for highly curved small vessels and to keep the algorithm computationally efficient.

• CONCLUSION

Low vessel-background contrast causes some of the small vessels to lose their visibility in MIP images. A cylinder model was developed to simulate a three-dimensional MR angiogram. A vessel enhancement filter, G^1_3, using long-range signal correlation was presented. The results of applying the G^1_3 vessel enhancement filter in three-dimensional MRAs demonstrate that this filter suppresses background signal and image noise more effectively compared with the maximum-minimum filter and cross-section filter reported in Du et al. (12). One study has shown that the G^1_3 filter increases the vessel-background CNR by a factor of 2.52 compared with the maximum-minimum filter and by a factor of 3.51 compared with the cross-section filter.

Acknowledgments: We thank the Biodynamics Research Unit of the Mayo Foundation for use of the Analyze software package.

References

1. Laub G. Displays for MR angiography. Magn Reson Med 1990; 14:222–229.
2. Anderson CM, Saloner D, Tsuruda JS, Shapeero LG, Lee RE. Artifacts in maximum-intensity-projection display of MR angiograms. AJR Am J Roentgenol 1990; 154: 623–629.
3. Brown DG, Riederer SJ. Contrast-to-noise ratios in maximum intensity projection image. Magn Reson Med 1992; 23:130–137.
4. Parker DL, Haacke EM. Signa-to-noise, contrast-to-noise, and resolution. In: Potchen EJ, Haacke EM, Siebert JE, and Gottschalk A, eds. MRI angiography. St. Louis: Mosby-Year Book, 1993; 66–79.
5. Vandermeulen D, Delaere D, Suetens P, Bosmans H, Marchal G. Local filtering and global optimization methods for 3D magnetic resonance angiography (MRA) image enhancement. In: Visualization in biomedical computing. SPIE 1992; 1808:274–288.
6. Gerig G, Kubler O, Kikinis R, Jolesz FA. Nonlinear anisotropic filtering of MRI data. IEEE Trans Med Imaging 1992; 11:221–232.
7. Chen H, Hale J. An algorithm for MR angiography image enhancement. Magn Reson Med 1995; 33:534–540.
8. Klose U, Petersen D, Martos J. Tracking of cerebral vessels in MR angiography after highpass filtering. Magn Reson Imaging 1985; 13:45–51.
9. Ehricke HH, Donner K, Koller W, Straßer W. Visualization of vasculature from volume data. Comput Graphics 1994; 18:395–406.
10. Lin W, Haacke EM, Masaryk TJ, Smith AS. Automated local maximum-intensity projection with three-dimensional vessel tracking. J Magn Reson Imaging 1992; 2: 519–526.
11. Du YP, Parker DL, Davis WL. Vessel enhancement filtering in 3D MR angiography (abstract). In: Proceedings of the Society of Magnetic Resonance in Medicine. Berkeley: Society of Magnetic Resonance in Medicine 1993; 454.
12. Du YP, Parker DL, Davis WL. Vessel enhancement filtering in three-dimensional MR angiography. J Magn Reson Imaging 1995; 5:353–359.
13. Du YP, Parker DL. Digital vessel-enhancement filtering in three-dimensional MR angiograms using long range signal correlation (abstract). In: Proceedings of Society of Magnetic Resonance in Medicine 1995; 581.
14. Hylton NM, Simovsky I, Li AJ, Hale JD. Impact of section doubling on MR angiography. Radiology 1992; 185:899–902.
15. Saloner D, van Tyen R, Hanson W. Image and object registry and connected voxel algorithms for display of MRA vessel signal (abstract). In: Book of abstracts: Society of Magnetic Resonance in Medicine 1992. Berkeley: Society of Magnetic Resonance in Medicine 1992; 476.
16. Du YP, Parker DL, Davis WL. Band-limited interpolation in MR angiography (abstract). In: Proceedings of the Society of Magnetic Resonance in Medicine. Berkeley: Society of Magnetic Resonance in Medicine 1993; 704.
17. Du YP, Parker DL, Davis WL, G. Cao. Reduction of partial-volume artifacts using zero-filled interpolation in 3D MR angiography. J Magn Reson Imaging 1994; 4:733–741.
18. Parker DL, Du YP, Davis WL. The voxel sensitivity function in Fourier transform imaging: applications to magnetic resonance angiography. Magn Reson Med 1995; 33:156–162.
19. Du YP, Parker DL, Davis WL, Blatter DD. Contrast-to-noise ratio measurements in three-dimensional magnetic resonance angiography. Invest Radiology 1992; 28:1004–1009

Erratum

The article by Yiping P. Du and Dennis L. Parker entitled Vessel Enhancement Filtering in Three-Dimensional MR Angiograms Using Long-Range Signal Correlation, which appeared on pages 447–450 in JMRI Volume 7, Number 2, contained an inaccuracy in the text accompanying Equation [3]. The equation and text should have appeared as follows:

$$G_M^K(l) = \max_{j=1,\ldots,19} \left(\sum_{k=-K}^{K} g_{(l+kJ),M} \right) \qquad (3)$$

where $\sum_{k=-K}^{K} g_{(l+kJ),M}$ is the summation of $g_{l,M}$ along the direction of J.

The error is regretted.